LAWRENCE
LIVERMORE
NATIONAL
LABORATORY

UCRL-JRNL-203479

Nonlinear mixing behavior of the three-dimensional Rayleigh-Taylor instability at a decelerating interface.

H.F. Robey, B.A. Remington, M.J. Edwards, T.S. Perry, R. J. Wallace, H. Louis, R.P. Drake, D. L. Leibrandt, E. C. Harding, C. C. Kuranz, M. Blackburn, J. P. Knauer

April 9, 2004

Physics of Plasmas

Disclaimer

UCRL-JRNL-203479

Nonlinear mixing behavior of the three-dimensional Rayleigh-Taylor instability at a decelerating interface

R.P. Drake, D.L. Leibrandt, E.C. Harding, C.C. Kuranz, M. Blackburn

University of Michigan

H.F. Robey, B.A. Remington, M.J. Edwards, T.S. Perry, R.J. Wallace, H. Louis,

Lawrence Livermore National Laboratory

J.P. Knauer, *University of Rochester*

ABSTRACT

We report results from the first experiments to explore the evolution of the Rayleigh-Taylor (RT) instability from intentionally three-dimensional (3D) initial conditions at an embedded, decelerating interface in a high-Reynolds-number flow. The experiments used ~ 5 kJ of laser energy to produce a blast wave in polyimide and/or brominated plastic having an initial pressure of ~ 50 Mbars. This blast wave shocked and then decelerated the perturbed interface between first material and a lower-density, C foam. This caused the formation of a decelerating interface with an Atwood number ~2/3, producing a long-term positive growth rate for the RT instability. The initial perturbations were a 3D perturbation in an "egg-crate" pattern with feature spacings of 71 μm in two orthogonal directions and peak-to-valley amplitudes of 5 μm. The resulting RT spikes were observed to overtake the shock waves at the undisturbed, "free-fall" rate, and to subsequently deliver material from behind the interface to the forward shock. This result is unanticipated by prior simulations and models.

I. INTRODUCTION

The Rayleigh-Taylor (RT) instability[1, 2] is a ubiquitous phenomenon, having consequences in the dynamics of atmospheric circulation, in laboratory fluids and gasses, in magnetized plasmas from those produced for fusion to planetary magnetospheres, and in supernovae, to name only a few. This ubiquity has made RT a subject of extensive study, leading to hundreds of published papers in the last decade alone. It is not surprising that there are many specific regimes of RT, corresponding to specific aspects of various physical systems such as surface tension or granularity. Our focus here is on experiments to explore the behavior of the RT instability, developing from initial conditions with three-dimensional (3D) structure, at interfaces that are shocked and then decelerated by blast waves of high Mach number, in compressible flows of very high Reynolds number. This is the regime of interest to astrophysical phenomena such as supernovae, and accessible in the laboratory only by high-energy-density experimental techniques. The experiments we report were motivated by the desire to observe the evolution of RT from initial conditions with 3D structure, including the transition to broadband fluid turbulence. We have observed the development of complex 3D structures that transport denser material through less dense material faster than standard models would predict.

In all environments, the RT instability causes regions of less-dense, buoyant material, known as “bubbles”, to float upward, and regions of more-dense, “heavy” material, known as “spikes”, to plunge downward. Both of these structures experience drag, which causes the “bubble head” and “spike tips” at their ends to broaden, often leading to Kelvin-Helmholtz instabilities. There has been partial success at modeling RT

using models based on the competition between buoyancy and drag. The vast majority of work on RT has explored the development of the instability from two-dimensional (2D) initial conditions, such as the sinusoidal undulation of an interface. This is the most straightforward situation to produce, to diagnose, and to simulate. In the realm of high-energy-density systems, this has included many studies of RT behavior at an ablation surface,[3-5] motivated by inertial fusion, and a number of studies[6-14] of RT behavior at a decelerating, embedded interface, motivated by basic science and/or astrophysics. In recent work with decelerating-interface experiments, buoyancy-drag models have proven successful, after adjusting for compressibility effects, in explaining observations with single-mode perturbations and 2D simulations have proven able to reproduce, on the whole, observations with 2D multimode perturbations.[15]

In addition, simulations of complex astrophysical phenomena remain largely 2D. Thus, for example Figure 1b shows results of a 2D simulation of the explosion of SN 1987A (Kifonidis, Max Planck Garching, private communication), obtained as part of a study of the role of neutrino-driven convection in this explosion.[16] One sees well-developed RT spikes of material from the interior of the star, penetrating through the He layer toward the He-H interface. The shear along the edges of these RT spikes drives the Kelvin-Helmholtz instability, which produces the observed roll ups. One significant question in the context of these simulations how RT would differ in 3D, and in particular how quickly it might deliver matter from the interior to the He-H interface. This happens later in the work of Kifonidis than in some earlier 2D simulations.[17] The timing matters because it determines whether the interior matter gets stuck behind the He-H interface or

penetrates far beyond it. Only the latter would be consistent with the observations (on the assumption of a globally symmetric explosion).

A second significant question in the context of these simulations involves the comparison of Figure 1a and Figure 1b, and is related to the onset of fluid turbulence. In experiments with fluids and gasses, such systems have at times evolved to a state of broadband turbulence. This is believed to require the intermediate development of 3D structure, as is clearly required in jets. It appears that a necessary condition for this transition[18] is that the "Reynolds number" must exceed about 30,000. The Reynolds number, *Re*, is defined as UL/ν, where U is the velocity difference across the flow, L is the spatial scale of the variations in the flow, and ν is the kinematic viscosity.[19] Such interfacial turbulence has a number of features. It transports matter and heat at a rate that is far more rapid than would be produced by molecular diffusion. It includes fluctuations of the interface that are three-dimensional and that span a wide range of spatial scales. There may be an "inertial range", in which energy is transported to smaller scales by the interaction of the turbulent motions (some authors consider this a defining feature). The notion that a system to be turbulent must have lost all trace of its initial conditions is appealing but may not be holding up.[20]

Moreover, simulations cannot clarify whether a system with a plasma interface becomes turbulent, and can even be misleading. Figure 1a shows the results of a laboratory experiment involving the evolution of a jet in which a high-velocity fluid penetrates a second fluid at $Re \sim 30{,}000$. One can see the evolution of the Kelvin-Helmholtz instability along the surface of the jet, followed by the appearance of modulations in three dimensions around the jet, to a phase characterized by the growth of

an apparently homogenous turbulent region containing fluctuations at many scales. Figure 1b, in contrast, does not develop such a turbulent region. This is not surprising as the spikes in the simulation have a Reynolds number of a few thousand, due to numerical viscosity, and are also 2D. However, the Reynolds number of the spikes in the actual, 3D supernova explosion exceeds 10^{10}. Thus, it seems likely that the actual transport of material in the supernova explosion could be quite different from that seen in Figure 1b. Both the astrophysical applications and the limitations of simulations motivate experiments to produce turbulence at interfaces in plasmas.

In the literature, there is only limited work on RT in 3D, high-*Re* systems. The simulations have either been focused on the behavior of isolated bubbles or spikes[21-23] or or on multimode phenomena in thin, ablative layers relevant to inertial fusion.[24] There is to our knowledge only one exploration by detailed simulations in 3D of multimode RT at an embedded interface,[25] but it is a calculation for incompressible fluids at low *Re*. The only 3D experiments were focused on RT at an ablation layer,[26] again motivated by inertial fusion. In contrast, the 3D experimental work in low-Re, low-Mach-number systems is too vast to cite. We mention here only that of Dimonte and Schneider,[27] which has had a significant impact on recent theoretical work.

II. EXPERIMENTAL CONFIGURATION AND CONDITIONS

A. Target Structure

Figure 2 is a cross-sectional diagram of the target used for these experiments. The drive lasers irradiate a polyimide surface, 800 μm in diameter. The polyimide used has chemical structure $C_{22}H_{10}O_5N_2$ and a density of 1.41 g/cm^3. It is 150 μm thick. At the rear

surface a 200 μm wide, 75-μm deep slot has been milled in the polyimide. A strip of $C_{500}H_{457}Br_{43}$, of density 1.42 g/cm^3, has been glued into the slot. These two materials were chosen to have nearly the same density and to be dominantly low-Z, so that their hydrodynamic response to pressures of tens of Mbars would be similar. The role of the strip is to provide a thin layer that more strongly absorbs the x-rays used to radiograph the target during the experiment, so that one can observe the structure near the center of the surface without obscuration by edge effects. The rear surface of this assembly was then machined to produce the egg-crate structure shown in Figure 3. The amplitude of the pattern defined by the machining tool is $a_o \sin(\lambda_x x)\sin(\lambda_y y)$, with a_o = 2.5 μm and $\lambda_x = \lambda_y$ = 71 μm. One can see in the figure that tearing of the material during machining produced substantial additional structure of smaller amplitude and shorter wavelength. The potential significance of this is discussed below.

Beyond the initial plastic materials was a long cylinder of carbon foam, again 800 μm in diameter. The foam is carbon resorcinol formaldehyde. It has an open cell structure, with characteristic cell sizes of < 0.1 μm. The surfaces of the ends of the foam were planar, and were smoothed so that the surface finish is better than 1 μm. Foam densities of 50 mg/cm^3 and 100 mg/cm^3 were used in various experiments.

A Be shock tube, of 1100 μm outside diameter and 800 μm inside diameter held the cylindrical structures just described, and the driven end of the target included a shield of 2.5 mm diameter to protect the outer target structures from laser irradiation. Figure 2 includes a drawing of such a target. .

B. Laser Irradiation and Target Diagnostics

Ten beams of the Omega[28] laser irradiate the polyimide surface of the target at a wavelength of 0.35 μm. The laser pulses are of 1ns full width at half maximum (FWHM), with approximately 100 ps rise and fall times and approximately flat tops. The energy in each laser beam is typically 450 J (+/- 10%). Each beam passes through a distributed phase plate and a distributed polarization rotator, producing a spot with a smooth overall profile and fine speckles on a 5-μm scale. The combined intensity profile of the 10 beams has a broad maximum with a 800 μm FWHM, so that the average irradiance is 9×10^{14} W/cm^2. This irradiation produces an ablation pressure of approximately 50 Mbars (based on simulations that match the velocity of the shock wave produced). Because shock waves anneal rapidly, the fine-scale modulations in the irradiance will not produce structure in the shock when it reaches the rear of the target. The shock wave remains within the dense plastic layer when the laser turns off, after which a rarefaction from the front surface of the target overtakes the shock wave shortly before it breaks out of the plastic. This produces the desired blast-wave structure, with an abrupt acceleration by the shock followed by an extended deceleration in the rarefaction.

The role of preheat in these experiments remains incompletely explored, and is a topic for future research. The laser irradiation produces both x-rays and electrons that penetrate the target and heat the interface before it is reached by the shock. The x-ray preheat is calculated, in the simulations described below, to heat the interface to a temperature of 0.3 eV and produce about 2 μm of motion before the shock arrives. The amount and spectrum of the energetic electrons is not well known. They potentially could have a larger effect, but experiments will be needed to quantify this. The essential impact

of any preheat is to alter the initial conditions that are encountered by the shock. This could certainly affect the detailed structures present in the deep nonlinear regime, but seems unlikely to have a dominant effect on the onset of turbulence or the overall spike penetration.

The principal diagnostic of these experiments is x-ray radiography. Several additional laser beams irradiate both sides of a thin metal target, typically Sc, located approximately 4 mm from the shock tube, as is shown in Figure 4. The properties of these beams are nearly identical to those of the drive beams, although they are at times focused without phase plates to a somewhat smaller spot. These backlighter beams are delayed by 10 to 30 ns relative to the drive beam, so that they can detect the interface after it has evolved over some distance. The x-ray radiation at several keV, which is dominated by the K_α radiation (at 4.3 keV for Sc), passes through the target, is imaged by an array of 16 pinholes, and is detected by a gated detector.[29] The 16 images are offset slightly in time, being distributed within the 1 ns backlighter pulse, but the evolution is gradual enough that they are effectively simultaneous. A gold grid, mounted to the target, provides a calibration of both location and magnification.

C. Experimental Conditions

Given the limited ability to diagnose these dense plasmas, we are forced to rely on simulations for an assessment of some experimental parameters. For this purpose, we used the HYADES code,[30] a one-dimensional (1D), Lagrangian, single-fluid, three-temperature code with multigroup diffusive radiation transport. It is well known (D. Braun, private communication) that such 1D simulations, run with the actual laser intensity, produce too large an ablation pressure in consequence of their ignorance of

lateral heat transport. By comparison with previous experiments, we determined that using an irradiance of 4.2 x 10^{14} W/cm^2 in the simulation produces shock and interface motions that are generally consistent with observations.

The shock wave produced by the laser propagates through half the dense plastic (the polyimide layer) before the laser pulse ends, after which the front-surface rarefaction overtakes the shock to form a blast wave, before the shock reaches the plastic-foam interface. When the blast wave reaches the interface, the dense plasma in the plastic rarefies, launching a shock into the foam, initially at ~100 km/s. The velocity of the interface is nearly 80 km/s at first, decreasing to ~ 40 km/s by 20 ns. This deceleration creates a positive growth rate for the Rayleigh-Taylor instability. Figure 4 shows results from a 1D simulation that reproduces the timing and velocity of the shock wave until 17 ns in the experiment. At 17 ns, the peak pressure produced by the shock wave has been reduced to ~1 Mbar, and the post-shock temperature in the plasma is ~ 15 eV, for the case of a 50 mg/cm^3 foam. The shock velocity is 60 km/s.

One can see in Figure 4 the typical structure that develops when a blast wave crosses an interface at which the density decreases. A forward shock propagates into the low-density material, producing compression, acceleration, and heating. The decrease in density, velocity, and pressure behind this shock is characteristic of decelerating shock waves. (The profiles would be flat in a steady shock wave.) The interface with the plastic is quite evident in the density and temperature. Further to the left is the reverse shock, evident in all four variables. This shock does not form immediately when the blast wave crosses the interface (which is why it is not designated a “reflected shock”). Instead, it evolves over time as the pressure in the incoming plasma from the blast wave decreases

more rapidly than the pressure in the material just behind the decelerating interface. There is only a very gradual decrease in the density and pressure of the material between the two shocks. The shocked foam layer expands very little on the timescale of the experiment, while the shocked plastic layer expands during its initial rarefaction, and less after that. Further to the left, in the plasma that is flowing toward the reverse shock, there is a perturbation in density and change in temperature associated with the transition from polyimide to CHBr. The difference in the equation of state tables used for these two materials is responsible for this (the difference in initial density is < 1%). This perturbation might or might not be real.

Based on simulations of very similar experiments, Robey et al. evaluated[14] the kinematic viscosity, concluding that it is approximately 0.05 cm^2/s in the foam and 0.1 cm^2/s in the plastic, while the coefficient for mass diffusion by binary collisions is 0.08 cm^2/s. Thus, for a 35 μm radius spike, and a shear velocity along the spike of 10 km/s (see below), one has a Reynolds number, *Re*, that is ~ 7×10^4. (If one chose to use the entire mix layer thickness to evaluate *Re*, it would be larger.) Such a system, if sustained long enough, seems a good candidate for the production of a turbulent state. In contrast, binary diffusion is negligible. On a 30 ns timescale one would expect the smearing of interfaces by binary diffusion to be of order 1 μm.

III. EXPERIMENTAL RESULTS

The principal data from these experiments were radiographic images obtained at selected times. The framing camera produced up to 16 images separated in time by up to 800 ps. In most cases the signal-to-noise of these images could be improved by adding them. The fluid motion at ~ 45 km/s produces a horizontal smearing of 36 μm due to this

motion. In theory this could degrade the resolution of the image from the fundamental limit of 10 μm due to the pinhole. In practice, the noise from local gain variations in the framing camera combined with the limited x-ray flux precludes one from attaining this resolution, so that averaging the images produces better results. In the images, the spatial scale is defined so that the front surface of the target is at 0 μm in *x* and the axis of the target is at 0 μm in *y*. The foam material thus begins at 150 μm.

Figure 5a-5c shows three images from experiments using 50 mg/cm^3 foam. Some experimental details deserve mention. The color scale on these images has been adjusted to provide the best possible view of the structures near the interface. Other features, such as the fiducial grid in the upper right corners and the dense material between the reverse shock and the interface, are resolved in the data though not very visible in this presentation of it. The fiducial grid was measured before the experiment and used to calibrate the magnification and location of the image. The images are recorded on active strips of limited width. This produces the dark areas where there is no signal at the lower left and upper right of the images shown. In addition, a flaw in the detector on one image produces the dark dot on the image and the continuation of some images past the ends of the active strip contributes linear changes in brightness toward the left of two of the images.

Next consider the physical features seen in these images. There is a bright region toward the left. This is the low-density material flowing toward the reverse shock, which is evident as an abrupt decrease in intensity. The reverse shock is much less well defined by 21 ns, as by then the instability has led to modulation of the entire layer of dense plastic. Moving to the right, the plastic-foam interface is not a simple one because of the

action of the instability. One can see a series of alternating bright and dark features, which we attribute to the presence of bubbles of foam material interspersed with spikes of CHBr. From these images, it is not so obvious where the left edge of the bubbles (the "heads") may be. In fact, the dense plastic material has become modulated through the development of the instability. Thus, a vertical Fourier transform of these images shows modulations at the imposed wavelength that extend some distance into the dense material. This may be most evident visually in the image at 17 ns. By 21 ns, the dense material is becoming more globally modulated. One can determine the location of the bubble heads fairly accurately, however, by examining narrow horizontal slices through the image. One sees an abrupt decrease in signal where the foam ends and the CHBr begins. We used this approach to determine the location of the bubble heads, and of the other experimental features, for the analysis below.

Continuing to the right, there is a very structured layer, the "mix layer", that we will discuss further shortly. In the image at 13 ns, the shock wave in the foam is present about 100 μm beyond the end of the spikes. This is very difficult to see in the image as shown, but it is present as was also confirmed by separate measurements using targets with unperturbed, planar interfaces. By 17 ns the mix layer has extended to the location of the shock and this remains the case at 21 ns.

Now consider the structure in the mix layer. In typical data and simulations of Rayleigh-Taylor in compressible media affected by strong shocks, nearly all of which are either two-dimensional or concerned with the behavior of a single spike, one sees distinct spikes that develop enlarged tips which roll up due to the Kelvin-Helmholtz instability. Indeed, data at 10 ns (with 100 mg/cc foam) shows this same behavior in the present

experiments. But this is not what one sees here. Instead, one sees two sets of spikes that are out of phase with one another. This is present in all three of the images shown here, and may be most evident in the image at 21 ns, where there are four particularly transparent bubbles in two pairs that are offset laterally relative to the flow. The fact that the spikes overtake the shock is also unusual, and is also discussed further below.

Figure 5d-5f shows the vertical fast Fourier transforms (FFTs) from the images shown above the FFTs. The display has been adjusted here so that all features present above noise are visible, so comparisons of intensity across images are not meaningful. There are very clear signals in the mix layer, centered at wavelengths somewhat greater than 50 μm and 100 μm. Overall, one can see a general trend at the later times toward longer wavelength, and toward increased complexity. The trends seen are consistent with the pattern shown in Fig. 3. In various images, the signals near 50 μm wavelength in the FFT vary in strength relative to the signals near 100 μm wavelength. This may reflect the placement of the spikes on the CHBr strip. The EOS of polymide and CHBr is not identical, and the surface of the CHBr may be displaced by as much as 4 μm relative to the surface of the polyimide (because of the difference in the response of the two materials to machining). As a result, spikes near the edge of the strip may be affected and do not necessarily remain as compact as those further from the edge. The result would be that alternating lines of sight measure through two well-formed spikes and then through only one. In projection onto the viewing direction, these lines of sight are spaced 50 μm, but their separation increases as the structures expand laterally.

Before interpreting these data, it is useful to quantify the hydrodynamic evolution of this system. Figure 6 shows some aspects of the hydrodynamic evolution, for the 50

mg/cm^3 data. The solid curve shows the interface position calculated by the simulations. The observed interface motion, in experiments with a planar interface, is consistent with the simulation. The average of the spike and bubble positions also moves with the interface location. This would not necessarily be expected or required; it indicates that in this case the mix layer is roughly symmetric about the original interface position. (This is after the rarefaction of the dense plastic.) A dashed line shows the simulated location of the shock wave. The data regarding the shock wave location are from experiments with or without a modulated interface. At the earliest time shown (and at 10 ns for 100 mg/cm^3 foam), the data and the simulation agree on the shock location. At 17 ns the picture is mixed. In one case, the shock-wave location lies on the simulation result. In another case, both the shock and the average position of the bubbles and spikes lie below those of the simulation. The laser energy was not anomalously low. We can assess the metrology from photographs, and any error was much smaller than would be needed to make up the observed difference. By 21 ns, the shock wave has slowed significantly in comparison with the value in the simulation. There are least two possible causes of this. On the one hand, the shock becomes curved by this time, and 2D simulations show that the curved shock slows (presumably due to the lateral transport of energy and momentum). On the other hand, the slowing of the shock is simultaneous with the development of an additional absorption feature just behind the shock, and may correspond to a transition of the foam equation of state as pressure decreases. One hypothesis is that the foam may transition into a regime where it crushes before it heats and fully ionizes. Such a transition would not be in the tables used by the simulations.

A second measure of the hydrodynamic behavior is the evolution of the mix layer itself. Figure 7 shows the separation of the bubble heads and spike tips as a function of time in the experiments, with a line at 10 km/s shown for comparison. The latest data point, at 26 ns, shows the distance between the modulated surface of the dense plastic (taken to be bubble heads or remnants thereof) and the shock, as no intermediate structures are resolved at that time. Recall that the initial amplitude of the perturbation was 5 μm, already large enough that one would anticipate no linear-instability phase with exponential growth. In both sets of data there is clearly a more than linear increase in the mix-layer depth with time, until the rate of growth slows after the spikes reach the shock and as the shock stalls. The expansion of the mix layer contributes some of the observed growth. The amount of expansion is always small in the shocked foam, being no more than 10% at 10 ns and 20% at 20 ns. The region of plastic containing the bubbles has expanded by a factor of about 3 due to the rarefaction but changes only 20% between 10 ns and 20 ns. The fact that the growth between the first two data points for each foam type is greater than the average up to that point shows that unstable behavior, rather than decompression, produces the observed rapid growth.

The following sequence of events is seen in the data. First, there is a period during which the spikes and bubbles become larger. Next, there is a change in the morphology of the mix layer as a second set of spikes, out of phase with the first, forms. Considering Figures 5 and 6 shows that this shift in phase occurs approximately at the location of the unperturbed interface. After that, the mix layer grows rapidly and overtakes the shock. (This occurs first in the case of Fig. 5b for 50 mg/cm^3 foam, which is unfortunately the experiment with anomalously small shock and interface displacements, but also occurs at

13 ns for 100 mg/cm^3 foam, in an experiment whose shock and interface displacements are consistent with simulations.) The spikes subsequently deliver dense plastic material to the shock. Specifically, the absorption feature at the shock has 12 % absorption and is 20 μm wide with a planar interface, increasing to 19 % absorption and 50 μm wide for the modulated case of Fig. 5c.

IV. DISCUSSION

The first conclusion from the data is that the spike growth seems quite rapid. This rapid growth of the spikes in the data leads one to ask whether or not their behavior is consistent with the buoyancy-drag models often used to describe RT turbulence, and fairly successful at describing the mix-layer growth for two-dimensional perturbations.[15] It makes sense here to examine the growth of the spikes as we can determine this more accurately because expansion is not an essential aspect. In addition, one might hope the model would be more accurate for the spikes, as during their evolution there is little compression and the theory is formally for incompressible fluids. We examined the implications of a standard 3D buoyancy-drag equation for the spikes,

$$\frac{du}{dt} = -Ag - \frac{(1-A)}{2} ku^2, \tag{1}$$

in which u is the time-derivative of the distance from the spikes to the interface, g is the acceleration of the interface (which is negative, causing slowing), and k is the wavenumber of the perturbation. The Atwood number is designated by A and equals $(\rho_1 - \rho_2)/(\rho_1 + \rho_2)$, where ρ_1 and ρ_2 are the densities on the higher-density and lower-density sides of the interface, respectively. A is 2/3 here as the density drop is 5. We obtained Eq. 1 from Oron et al.,[31] but similar or identical equations are discussed in numerous papers,

reviewed by Dimonte.[32] A fit to the simulation of Fig. 6 gives $a = -6\ (t/4)^{-1.2}$, with a in μm/ns^2 and t in ns. Integrating Eq. 1, for a wavelength of 71 μm, produces the results shown in Figure 8. At 13 ns, the spikes have freely fallen nearly to the shock. After 13 ns the spikes are at the shock and their length is controlled by the shock. The significance of Fig. 8 is that *we are observing spike penetration that approximately equal to the free-fall distance over distances approaching 2 perturbation wavelengths*. This is both remarkable and unanticipated.

We should note that the analytic analyses have been limited to either single bubbles or large multimode statistical ensembles. We did note in the introduction that, and that the computational analysis is rather limited. The structure seen in the present data clearly does not correspond to the broadband, multimode turbulence that might lead one to see growth of the mix layer depth with time, t, proportional to $(1/2)\alpha\, at^2$, where a is the acceleration and α is a factor. However, there is some potential that the high-frequency modulations of the interface seen in Fig. 3 and/or the step at the edge of the tracer layer contribute in some way to the dynamics that produces such large spike penetrations.

The second conclusion relates to the observed change in spike morphology after 10 ns. The data, a two-dimensional projection of the spikes in the CHBr layer, show a shift in the spike location by 1/2 the spike spacing. One way this could arise is as follows. The nearest-neighbor spikes define an array of square patterns, with a symmetry axis at the center of each square. As the initial spike tips broaden, their ability to interact also increases. Suppose they interact so as to direct the flow of matter into new spikes emerging along the symmetry axis of each square. This would produce the observed data,

and might perhaps lead to an initial period of rapid growth in the second tier of spikes. One can imagine that this process could repeat itself again if the spikes had not overtaking the shock. (The increased drag on spikes that penetrate beyond the shock effectively prevents the spikes from emerging ahead of it.) Thus, one concludes that the rapid growth of the mixing layer and the changing spike morphology may possibly result from spike interactions. It is also possible that the differences in interaction of the alternating rows of spikes with the edge of the tracer strip contribute to the observed morphology, but it is not clear how this could produce very transparent bubbles lying directly below the spikes as in Fig. 5b.

The third conclusion relates to turbulence as traditionally defined. Because turbulence can lead to rapid increases in mass transport, one may wonder whether it could be playing a role here. Experimentally we cannot rule out the presence of structures on spatial scales below 10 μm. If there were structures, lateral to the mean flow, with scales from 10 μm to 30 μm, then we would expect to have seen them in the FFT. However, we did not (Figure 5 only displayed the range of wavelengths with some signal.) The spatial averaging along the line of sight certainly might smear out such structures, but as one is only seeing the edges of two spikes, this would be unlikely to remove all traces of it. One might anticipate that the Kelvin-Helmholtz instability could produce such structures. The shear velocity (Δu) along the spikes is above 10 km/s. Thus, for wavenumber k of order the inverse of the 35 μm width of the spike, the exponential growth rate for an abrupt shear layer ($k\Delta u$) corresponds to 6 e-foldings per ns. One infers that the velocity gradient across the shear layer is probably gentle enough to stabilize Kelvin-Helmholtz at such scales. In addition, even if turbulence were present throughout

the mix layer, one would anticipate mixing over only some fraction of the free-fall distance while here there seems to be a larger effect. Thus, it seems unlikely that small-scale turbulence is responsible for the observed growth of the mix layer.

The fourth conclusion from the data is a sensible consequence of the above but is also potentially important. As is indicated by the comparison of the size and depth of the absorption feature at the shock, once the spikes reach the shock it appears that the dense plastic material accumulates there. This accumulation will increase with time. Indeed, by 26 ns with 100 mg/cm^3 foam, the absorption feature has ~25% absorption and is 70 μm thick. For comparison, a single spike at 13 ns has ~ 5% absorption and is ~ 35 μm in radius. The consequences and indeed the precise causal factors remain to be determined, but it seems clear that under some circumstances the 3D Rayleigh-Taylor instability can deliver significant amounts of material to the forward shock. This could produce much more rapid transport of material in laboratory and astrophysical systems than one would otherwise expect. The implications of this could be dramatic, but their exploration is beyond the scope of the present paper.

V. FUTURE DIRECTIONS

The results discussed here and their apparent implications are sufficiently novel that careful, follow-up studies are warranted to determine what really happens to three-dimensional Rayleigh-Taylor instabilities. Experimentally, the measurements are definitely limited by both noise and contrast, so the development of improved diagnostic techniques, such as backlit pinhole measurements or curved-crystal imagers, would be of value, as would the development of higher-contrast tracer layers, such as iodine-doped plastic. Using either a dense gas or cryogenic hydrogen would also help, by removing

some of the uncertainties associated with foam crushing. It would be useful as well to obtain experiments of longer duration, but this would require producing higher-velocity blast waves. This might become feasible on NIF, but perhaps at the expense of complications from hot-electron preheat.

Computationally, the results motivate the use of the new generation of fast, adaptive hydrodynamic codes to evaluate 3D Rayleigh-Taylor behavior in compressible, strongly shocked systems. A systematic elucidation of the regimes of spike interactions remains to be attempted, and would provide valuable guidance to the interpretation of phenomena observed both in the laboratory and throughout the universe.

ACKNOWLEDGEMENTS

We acknowledge useful discussions with Aaron Miles, Dmitri Ryutov, and Dave Arnett, and useful technical contributions Mike Grosskopf, Amy Reighard, Leah Norstrund, and Kelly Korreck. We acknowledge the technical support of the target fabrication personnel at the Lawrence Livermore National Laboratory, and of the Omega Laser Operations team. Both were essential to the success of this work. Financial support for this work included funding from the U.S. Department of Energy to the University of Michigan under grants DE-FG03-99DP00284 and DE-FG03-00SF22021, and to the Lawrence Livermore National Laboratory under Contract No. W-7405-ENG48.

Work was performed in part under the auspices of the U.S. Department of Energy by the University of California, Lawrence Livermore National Laboratory under Contract No. W-7405-Eng-48.

REFERENCES

[1] L. Rayleigh, *Scientific papers ii* (Cambridge, Cambridge, England, 1900).

[2] S.G. Taylor, Proc. R. Soc. **A201**, 192 (1950).

[3] J.D. Kilkenny, S.G. Glendinning, S.W. Haan, B.A. Hammel, J.D. Lindl, et al., Phys. Plasmas **1**, 1379 (1994).

[4] C.J. Pawley, S.E. Bodner, J.P. Dahlburg, S.P. Obenschain, A.J. Schmitt, et al., Phys. Plasmas **6**, 565 (1999).

[5] J.P. Knauer, R. Betti, D.K. Bradley, T.R. Boehly, T.J.B. Collins, et al., Phys. Plasmas **7**, 338 (2000).

[6] K.S. Budil, B.A. Remington, T.A. Peyser, K.O. Mikaelian, P.L. Miller, et al., Phys. Rev. Lett. **76**, 4536 (1996).

[7] J. Kane, D. Arnett, B.A. Remington, S.G. Glendinning, J. Castor, et al., Ap. J. **478**, L75 (1997).

[8] J. Kane, D. Arnett, B.A. Remington, S.G. Glendinning, R. Wallace, et al., in *Second Oak Ridge Symposium on Atomic and Nuclear Astrophysics*, Oak Ridge, Tenessee, 1998).

[9] J. Kane, D. Arnett, B.A. Remington, S.G. Glendinning, G. Bazan, et al., Physics of Plasmas **6**, 2065 (1999).

[10] J. Kane, D. Arnett, B.A. Remington, S.G. Glendinning, G. Bazan, et al., Ap. J. Suppl. **127**, 365 (2000).

[11] J.O. Kane, H.F. Robey, B.A. Remington, R.P. Drake, J. Knauer, et al., Phys. Rev. E **63**, 055401R (2001).

[12] H.F. Robey, J.O. Kane, B.A. Remington, R.P. Drake, O.A. Hurricane, et al., Phys. Plasmas **8**, 2446 (2001).

[13] R.P. Drake, H.F. Robey, O.A. Hurricane, Y. Zhang, B.A. Remington, et al., Astrophys. J. **564**, 896 (2002).

[14] H.F. Robey, Y. Zhou, A.C. Buckingham, P. Keiter, B.A. Remington, et al., Phys. Plasmas **10**, 614 (2003).

[15] A. Miles, D. Braun, J. Edwards, H.F. Robey, R.P. Drake, et al., Phys. Plasmas, submitted (2003).

[16] K. Kifonidis, T. Plewa, H.-T. Janka, and E. Muller, ApJ Lett **531**, L123 (2000).

[17] B. Fryxell, E. Muller, and D. Arnett, Ap. J. **367**, 619 (1991).

[18] P.E. Dimotakis, J. Fluid Mech. **409**, 69 (2000).

[19] L.D. Landau and E.M. Lifshitz, *Fluid mechanics* (Pergamon Press, Oxford, 1987).

[20] A.W. Cook and P.E. Dimotakis, J. Fluid Mech **443**, 69 (2001).

[21] G. Tryggvason and S.O. Unverdi, Phys. Fluids A **2**, 656 (1990).

[22] J.P. Dahlburg, J.H. Gardner, G.D. Doolen, and S.W. Haan, Phys. Fluids B **5**, 571 (1993).

[23] J. Kane, D. Arnett, B.A. Remington, S.G. Glendinning, G. Bazan, et al., Ap. J. **528**, 989 (2000).

[24] J.P. Dahlburg, D.E. Fyfe, J.H. Gardner, S.W. Haan, and G.D. Doolen, Phys. Plasmas **2**, 2453 (1995).

[25] Y.-N. Young, H. Tufo, A. Dubey, and R. Rosner, J. Fluid Mech. **447**, 377 (2001).

[26] M.M. Marinak, B.A. Remington, S.V. Weber, R.E. Tipton, S.W. Haan, et al., Phys. Rev. Lett. **75**, 3677 (1995).

[27] G. Dimonte and M. Schneider, Phys. Rev. E **54**, 3740 (1996).

[28] T.R. Boehly, R.S. Craxton, T.H. Hinterman, J.H. Kelly, T.J. Kessler, et al., Rev. Sci. Intsr. **66**, 508 (1995).

[29] K.S. Budil, T.S. Perry, P.M. Bell, J.D. Hares, P.L. Miller, et al., Rev. Sci. Inst. **67**, 485 (1996).

[30] J.T. Larsen and S.M. Lane, J. Quant. Spectrosc. Radiat. Transfer **51**, 179 (1994).

[31] D. Oron, L. Arazi, D. Kartoon, A. Rikanati, U. Alon, et al., Phys. Plasmas **8**, 2883 (2001).

[32] G. Dimonte, Phys. Plasmas **7**, 2255 (2000).

FIGURE CAPTIONS

Figure 1. Comparison of (a) laboratory jet experiment with (b) two-dimensional simulation of SN 1987A during its explosion.

Figure 2. Target geometry for experiments.

Figure 3. Images of machined, perturbed surface of dense layer in target. (a) overview. (b) closeup showing mode structure and small-scale features.

Figure 4. Simulations of experiment during period of measurements discussed here. (a) density. (b) velocity. (c) pressure. (d) electron temperature.

Figure 5. Experimental data. (a), (b), and (c) show calibrated radiographic images at 13, 17, and 21 ns, respectively. Each of (d), (e), and (f) shows the one-dimensional FFT of a section of the image above it.

Figure 6. The simulated evolution of the interface (solid) and shock (dashed) locations is compared with results of measurements of interface location from targets with a planar initial interface (open squares), of the shock location (circles), and of the position midway between the bubble heads and spike tips (triangles). Error bars not shown are smaller than the symbols.

Figure 7. Growth of the mix layer, defined as the distance between the spike tips and the bubble heads. A line at 10 km/s is shown for comparison.

Figure 8. Spike growth and modeling. The solid line shows the spike length predicted by Eq. 1, while the dashed line shows distance from the free-fall line to the interface, both for 50 mg/cc foam. The triangles and solid dots show the spike length for 50 mg/cm^3 and 100 mg/cm^3 foam, respectively.

FIGURES

Figure 1

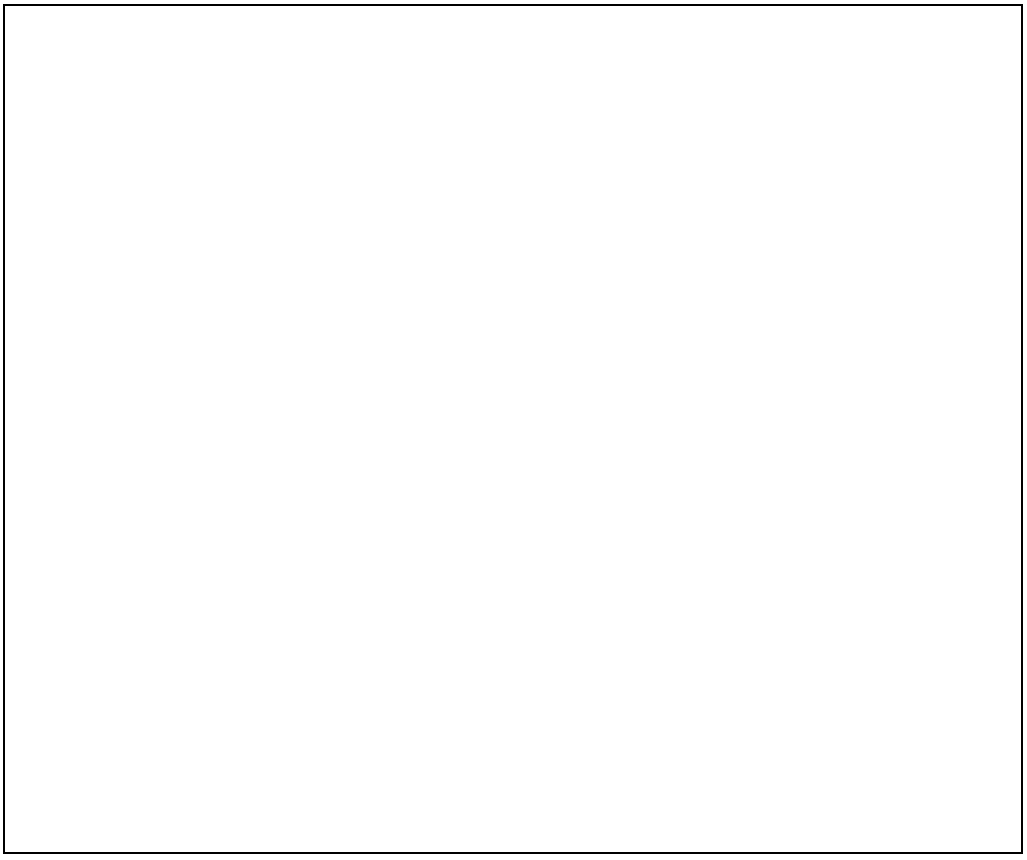

Figure 2

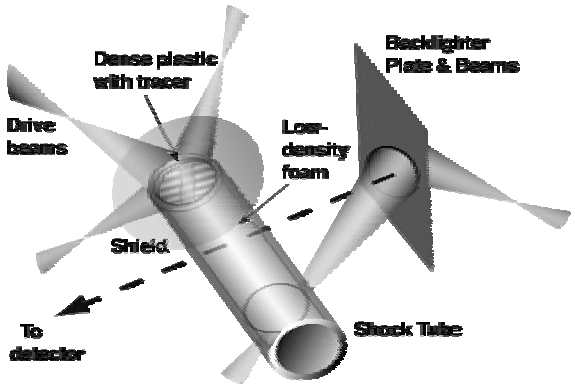
Dense plastic with tracer
Backlighter Plate & Beams
Drive beams
Low-density foam
Shield
To detector
Shock Tube

Figure 3

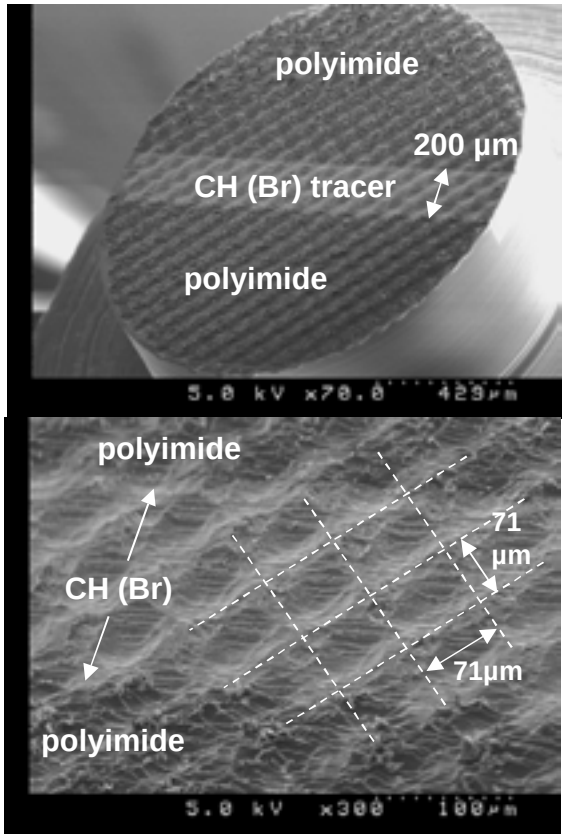
polyimide
200 µm
CH (Br) tracer
polyimide
5.0 kV x70.0 429µm
polyimide
71
µm
CH (Br)
71µm
polyimide
5.0 kV x300 100µm

Figure

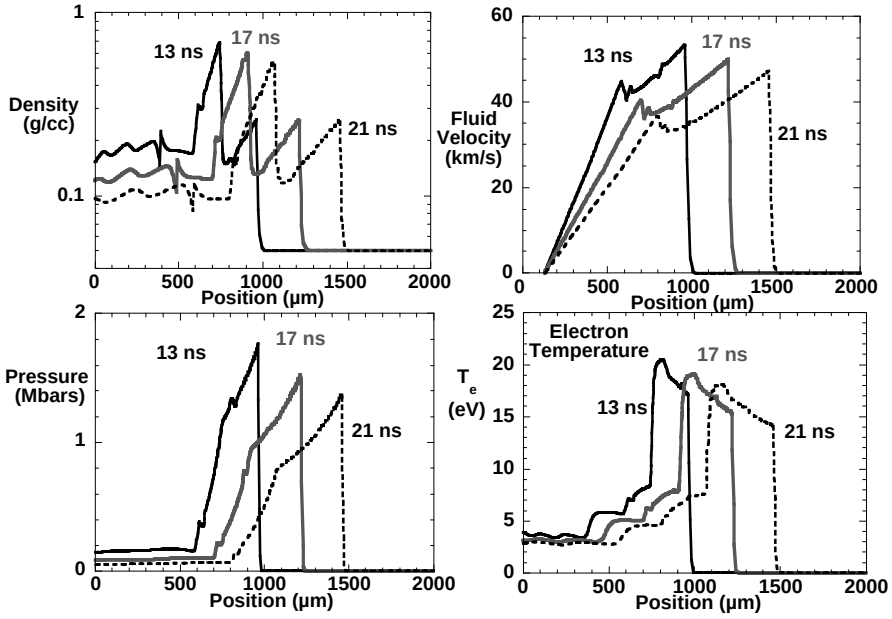
Density
(g/cc)
1
0.1
13 ns
17 ns
21 ns
0
500
1000
1500
2000
Position (μm)
Fluid
Velocity
(km/s)
60
40
20
0
Pressure
(Mbars)
2
1
0
Electron
Temperature
T
e
(eV)
25
20
15
10
5

Figure 5

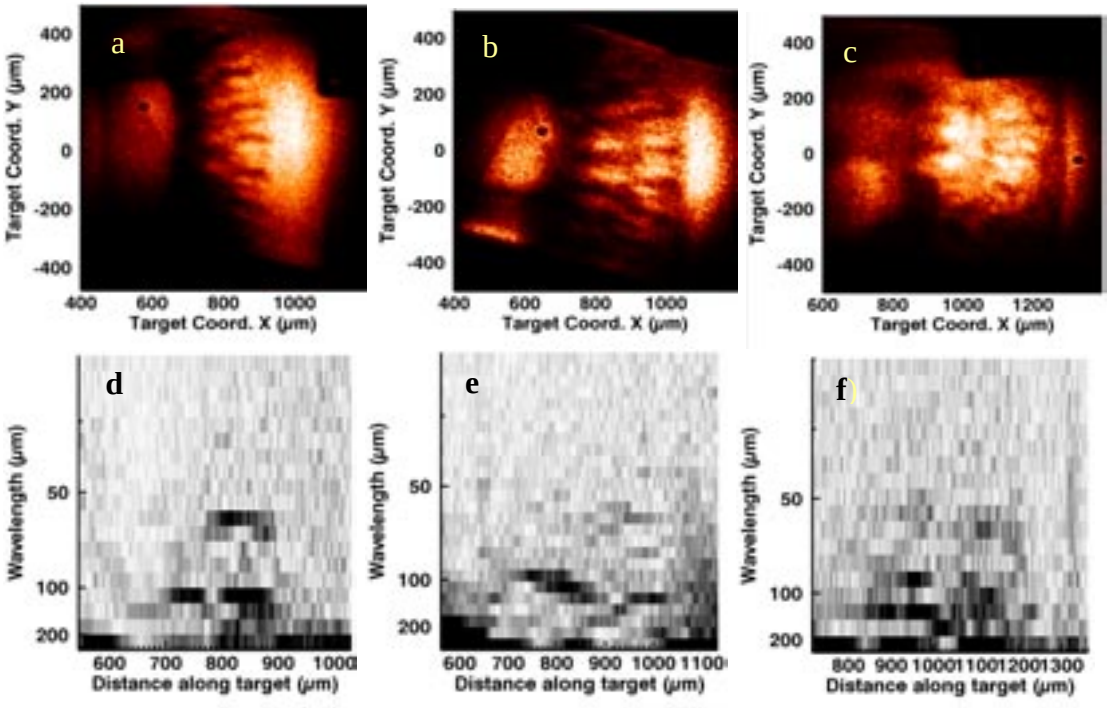
a
b
c
d
e
f
Target Coord. Y (μm)
Target Coord. X (μm)
Wavelength (μm)
Distance along target (μm)

Figure 6

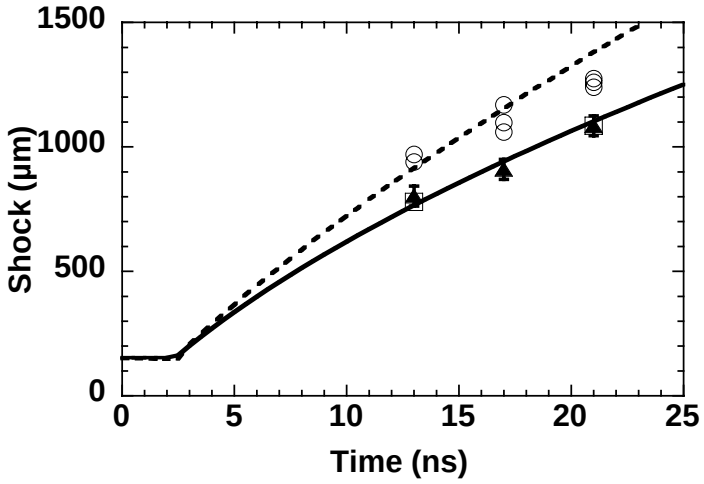

Figure 7

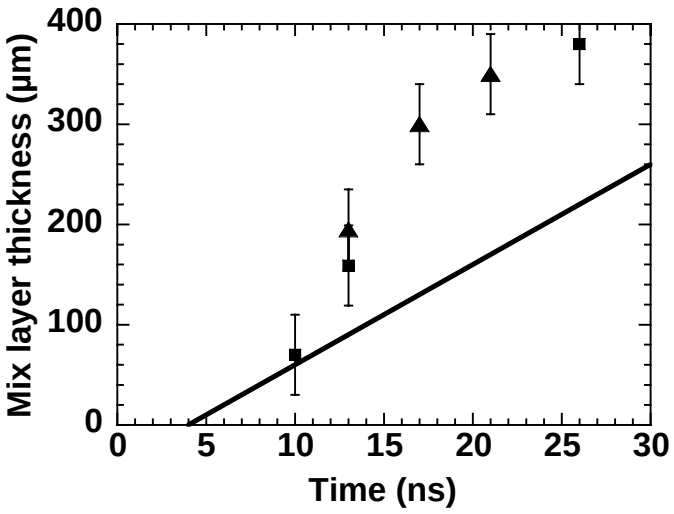
Mix layer thickness (μm)
400
300
200
100
0
0
5
10
15
20
25
30
Time (ns)

Figure 8

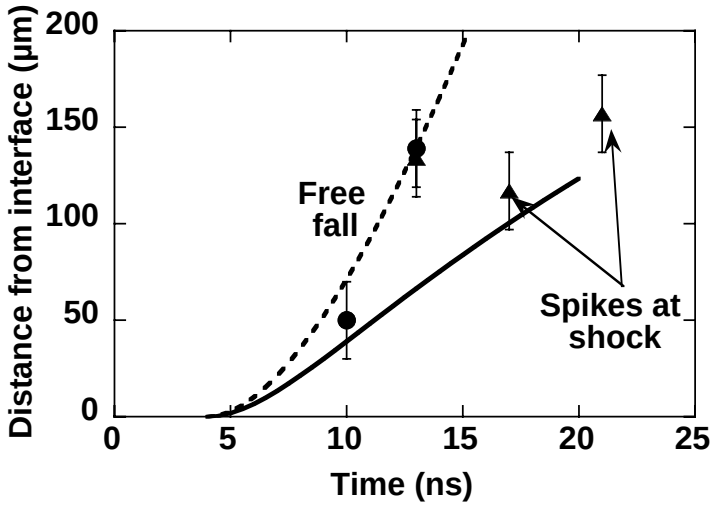
Distance from interface (μm)
200
150
100
50
0
0
5
10
15
20
25
Time (ns)
Free
fall
Spikes at
shock